Network Modeling and Operation Optimization of Electricity-HCNG-Integrated Energy System

Yue Qiu, *Student Member*, *IEEE*, Suyang Zhou, Wei Gu, *Senior Member*, *IEEE*, Yuping Lu, *Senior Member*, *IEEE*, Xiao-Ping Zhang, *Fellow*, *IEEE*, *Fellow CSEE*, Gaoyan Han, Kang Zhang, and Hongkun Lyu

***Abstract*—Hydrogen-enriched compressed natural gas (HCNG) has great potential for renewable energy and hydrogen utilization. However, injecting hydrogen into the natural gas network will change original fluid dynamics and complicate compressed gas's physical properties, threatening operational safety of the electricity-HCNG-integrated energy system (E-HCNG-IES). To resolve such problem, this paper investigates effect of HCNG on gas network dynamics and presents an improved HCNG network model, which embodies the influence of blending hydrogen on the pressure drop equation and line pack equation. In addition, an optimal dispatch model for the E-HCNG-IES, considering the "production-storage-blending-transportation-utilization" link of the HCNG supply chain, is also proposed. The dispatch model is converted into a mixed-integer second-order conic programming (MISOCP) problem using the second-order cone (SOC) relaxation and piecewise linearization techniques. An iterative algorithm is proposed based on the convex-concave procedure and bound-tightening method to obtain a tight solution. Finally, the proposed methodology is evaluated through two E-HCNG-IES numerical testbeds with different hydrogen volume fractions. Detailed operation analysis reveals that E-HCNG-IES can benefit from economic and environmental improvement with increased hydrogen volume fraction, despite declining energy delivery capacity and line pack flexibility.**

***Index Terms*—Electricity-HCNG-integrated energy system (E-HCNG-IES), hydrogen-enriched compressed natural gas (HCNG), improved HCNG network model, optimal dispatch.**

NOMENCLATURE

A. Abbreviations

WT, wt	Wind turbine.
PV, pv	Photovoltaic cell.
ELZ, elz	Electrolyzer.
CP, cp	Compressor.
MR, mr	Methanation reactor.
HS, hs	Hydrogen storage.
MZ, mz	Mixing zone.
GT, gt	Gas turbine.

B. Indices and Sets

N_t	Index set of dispatch period t.
Ω_{pipe}	Index set of pipeline ij in HCNG network.
Ω_{node}	Index set of node i/j in HCNG network.
Θ_{line}	Index set of power line nl in power network.
Θ_{bus}	Index set of bus n/l in power network.
N_w	Index set of gas source node w.

C. Cost Functions

$k_{om}^{wt/pv/elz/cp}$	Unit maintenance cost of WT/PV/ELZ/CP, \$/MWh, \$/m^3.
$k_{om}^{mr/hs/mz/gt}$	Unit maintenance cost of MR/HS/MZ/GT, \$/MWh, \$/m^3.
$k_{\text{wheel}}^{\text{grid}}$	Unit wheeling charge of public grid, \$/MWh.
$k_{\text{NG}}^{\text{buy}}$	Unit purchasing cost of natural gas, \$/m^3.
$k_{\text{HCNG},t}^{\text{buy}}$	Unit purchasing cost of HCNG, \$/m^3.
$penal_{wt/pv}^{\text{curt}}$	Unit penalty of wind/solar power curtailment.
$penal_{\text{CO}_2\text{NG}}$	Unit penalty of CO_2 emission.

D. Parameters

x	Abscissa of pipeline length.
L_i^G, L_n^E	Gas load of node i, and electric load of bus n, MW.
r_{HCNG}	Volumetric friction of hydrogen in HCNG.
λ_{ij}	Friction coefficient of pipeline ij.
D_{ij}	Diameter of pipeline ij, m.
A_{ij}	Sectional area of pipeline ij, m^2.
L_{ij}	Length of pipeline ij, m.
M	Gas molar mass, g/mol.
Z	Compressibility factor.
R	Gas constant, 8.31 (Pa·m^3)/(mol·K).
p_n, T_n	Standard pressure and temperature, Pa, K.
T	Gas temperature, K.
α	Coefficients of linear regression on Z, Pa^{-1}.
β	Coefficients of linear regression on Z.
$LHV_{\text{H/NG/HCNG}}$	Lower heat value of hydrogen/natural gas/HCNG, kWh/m^3.
$p_{\min/\max}$	Minimum/maximum node pressure, Pa.
$\tilde{q}_{\min/\max}$	Minimum/maximum pipeline flow rate, m^3/s.

Manuscript received November 9, 2022; revised December 8, 2022; accepted January 18, 2023. Date of online publication June 27, 2023; date of current version June 29, 2023. This work was supported in part by the Science and Technology Project of State Grid Corporation of China (No. 5100-202119574A-0-5-SF).

Y. Qiu, S. Y. Zhou (corresponding author, email: suyang.zhou@seu.edu.cn), W. Gu, and Y. P. Lu are with the School of Electrical Engineering, Southeast University, Nanjing 210096, China.

X. P. Zhang is with the School of Electronic Electrical and Systems Engineering, University of Birmingham, Birmingham, UK.

G. Y. Han, K. Zhang, and H. K. Lyu are with the Electric Power Research Institute of State Grid Zhejiang Electric Power Co., Ltd., Hangzhou 310014, China.

DOI: 10.17775/CSEEJPES.2022.07810

$\tilde{S}_{\min/\max}$	Minimum/maximum pipeline line pack, m^3.
$q_{w,\min/\max}$	Minimum/maximum injection of source node, m^3/s.
X_{nl}	Line reactance of line nl.
$F_{nl,\max}$	Line capacity of line nl, MW.
$P_{\max_{\text{grid}}}$	Line capacity of public grid, MW.
$ramp_{\min/\max_{gt}}$	Minimum/maximum ramping rate of GT, MW/h.
ρ_{air}	Air density, kg/m^3.
N_{wt}	Number of installed WT.
R_{wt}	Radius of installed WT.
A_{pv}	Installed area of PV.
ϑ_{pv}	Incidence angle of PV.
u_t	Wind speed at time t, m/s.
$\Re_t$	Solar radiation at time t, kWh/m^2.
$\eta_{wt/pv/elz/mr}$	Efficiency of WT/PV/ELZ/MR.
η_{MPPT}	Efficiency of MPPT.
$Cap_{gt/elz/mr/hs}$	Installed capacity of GT/ELZ/MR/HS, MW.
$\gamma_{cp/mr}$	Electricity consumption rate of CP/MR, kWh/m^2.
σ_{hs}	Self-release rate of HS.
$\eta_{hs,ch/dis}$	Charging/discharging efficiency of HS.
$\mu_{hs,\min/\max}$	Minimum/maximum storage state of HS.
$\gamma_{hs,ch/dis}$	Charge/discharge rate of HS.
$V_{\text{buy},\max_{\text{NG}}}$	Maximum purchasing natural gas flow rate, m^3/s.

E. Variables

ρ, v	Gas density and velocity.
$p_{i/j,t}$	Gas pressure at node i/j, Pa.
$q_{w,t}$	Gas injection of source node w, m^3/s.
$\tilde{q}_{ij,t}$	Average gas flow rate of pipeline ij, m^3/s.
$q_{ij,t}^{\text{in/out}}$	Inflow/outflow rate of pipeline ij, m^3/s.
$\tilde{S}_{ij,t}$	Average line pack of pipeline ij, m^3.
$\tilde{p}_{ij,t}$	Average gas pressure of pipeline ij, Pa.
$F_{nl,t}$	Power flow of line nl, MW.
$\theta_{n/l,t}$	Phase angle of bus n/l.
$P_{\text{grid},t}$	Power flow transmitted through upper grid, MW.
$P_{gt/wt/pv,t}$	Output electric power of GT/WT/PV, MW.
$P_{elz,t}$	Input electric power of ELZ, MW.
$V_{NG,mr,t}^{elz/hs}$	Natural gas flow produced from MR with hydrogen sources from ELZ/HS, m^3/s.
$V_{H,mr,t}^{elz/hs}$	Hydrogen injected into MR from ELZ/HS, m^3/s.
$V_{H,mz,t}^{elz/hs}$	Hydrogen injected into MZ from ELZ/HS, m^3/s.
$V_{H,hs,t}^{ch/dis}$	Hydrogen injected into/withdrawn from HS, m^3/s.
$V_{NG/H,t}^{\text{mix}}$	Natural gas/hydrogen flow rate injected into MZ, m^3/s.
$V_{NG,t}^{\text{buy}}$	Purchasing natural gas flow rate, m^3/s.
$V_{\text{HCNG},t}^{\text{buy}}$	Purchasing HCNG flow rate, m^3/s.

I. Introduction

A. Motivation

SINCE the industrial revolution, global air pollution and climate warming caused by massive consumption of fossil fuels have seriously threatened sustainable development of human society [1]. To reduce carbon emissions and dependence on fossil fuels in the energy field, new energy systems represented by integrated energy system (IES) and hydrogen energy system have attracted extensive attention in recent years [2], [3]. Hydrogen, as fuel and raw material, has a broad application prospect in the fields of power, heating, chemical industry, and transportation [4]. Various countries have launched evaluations of their hydrogen application prospects and set ambitious development goals, such as Japan, the US, the UK, Germany, France, China, and Russia [5]–[7].

The development of hydrogen depends on technical support of multiple links such as production, transmission, storage, and end-use [8]. However, lack of motivation for developing hydrogen production and storage facilities and high construction cost of hydrogen pipelines restrict the popularization and application of hydrogen [9]. Blending hydrogen with natural gas and injecting the hydrogen-enriched compressed natural gas (HCNG) into existing natural gas pipeline networks can help realize cross-regional transportation and utilization of hydrogen, which can break the dilemma of "chicken-and-egg" and effectively promote the large-scale consumption of renewable energy. Since 2004, demonstration projects including NaturalHy [10], Sustainable Ameland [11], HYREADY [12], and Chaoyang renewable hydrogen blending [13] have been launched successively, aiming to reveal the feasibility of transitional development of hydrogen energy in the form of HCNG.

To better accommodate renewable energy and achieve efficient coupling and conversion of hydrogen, electricity, and natural gas, it is urgent to explore implementation methods of HCNG application.

B. Literature Review

Due to the differences in physicochemical properties between hydrogen and natural gas, HCNG is bound to impact operating conditions of natural gas infrastructure [14], [15]. Existing research on HCNG mainly focuses on modeling, simulation, and gas flow analysis. Typically, plentiful tests have been carried out in real scenarios and simulation analysis with the help of SPS, pipeline studio, COMSOL multiphysics, ANSYS fluent, and other software [16], [17]. Authors of [17] performed a transient analysis of HCNG flow for a single pipe and looped network, respectively. The results show that increased hydrogen volume fraction will exacerbate pressure oscillation. In [18], the compressibility factor of HCNG was linearized under an isothermal steady-state, and the pressure drop equation of pipelines was also established. The influences of HCNG on gas flow rate, velocity, and node pressure were tested by simulation calculation. Li *et al*. proposed a computational fluid dynamics (CFD) approach to simulate and assess the dispersion of HCNG in the hydrogen-natural gas mixing station [19]. Obtained parameters of the flammable gas

cloud and dangerous area could be used to conduct a prior risk assessment and contingency planning of the mixing station. Reference [20] compared the effects of different hydrogen blending locations and modes on system operation status and verified the feasibility of HCNG to accommodate renewable energy. The effects of hydrogen blending fractions on the combustion and pollution of various engines were extensively investigated in [21] and [22].

Along with the urgent necessity of decarbonizing the energy system, research on IES containing hydrogen has recently been a research hotspot. In this paper, the electricity-HCNG-integrated energy system (E-HCNG-IES) is defined as an energy system that takes electricity and HCNG as core energy carriers to meet multi-energy demands of human production and living, as well as realize low-carbon and efficient consumption of fossil energy and renewable energy [23].

Currently, research on E-HCNG-IES focuses more on technical and economic analysis but less on planning and operation methods. Sensitivity and probability analysis were conducted in [24] to explore the feasibility of accommodating surplus renewable energy in China through HCNG transported by pipeline infrastructure. In this study, the ability of the HCNG project to reduce carbon emissions and increase revenue of renewable power plants was quantified. In [25], the Italian gas grid's capacity limits for consuming green hydrogen as a large-scale energy storage transport system were evaluated. Authors of [26] established a multi-stage flexible planning method for regional E-HCNG-IES considering the construction of energy stations and hydrogen-resistant retrofit of existing natural gas pipelines between sub-regions. A multi-period optimization approach for the hydrogen supply chain was presented in [8], revealing superiority of utilizing existing natural pipelines and byproduct hydrogen to decrease the average levelized costs of hydrogen. In IES operation optimization methods proposed in [27] and [28], hydrogen blending and co-combustion technologies were considered in the gas turbine model to facilitate renewable electricity. Reference [29] proposed an optimal operation method for IES incorporated with HCNG distribution networks based on comprehensive modelling of the hydrogen source, network, storage, and load.

Although the optimal operation approach for E-HCNG-IES is immature, existing research experience on modeling and operation optimization of integrated electricity and gas/hydrogen systems can provide meaningful references. Authors of [30] considered the uncertainty of renewable energy and load in the proposed electricity-hydrogen-gas-heat IES and established a stochastic optimal dispatching strategy based on improved spectral clustering. Reference [31] focused on the portfolio of hydrogen-related equipment and topology optimization of pipeline network problems, and the interaction between renewable energy, battery, power-to-hydrogen (P2H), and hydrogen commodity demand was analyzed in detail. Integrated demand response, power-to-gas (P2G)/P2H technology and hydrogen storage system were considered flexible resources of the multi-carrier energy hub proposed in [32], and a multi-objective stochastic dispatch method was formulated to verify economic-environmental benefits. Authors of [33] developed a three-stage distributionally robust chance-constrained model to jointly optimize the design and operation of IES equipped with power to hydrogen and heat (P2HH) technology. Deep reinforcement learning (DRL) methodology was adopted in [34] to solve the economic dispatch of IES considering wind power randomness and P2H. In addition, [35] constructed a framework called integrated energy sharing of hydrogen and electricity, considering the coupling effect of P2G devices and hybrid electric and hydrogen vehicles. The energy trade between different aggregators was solved by a distributed optimization method.

The research mentioned above reveals the significant role of hydrogen in the future energy system, while the dispatch approaches for E-HCNG-IES rarely consider the HCNG network's complex characteristics. It should be noted that the general flow equation is derived from the momentum equation based on a series of assumptions [36]. It and its simplified forms are widely used in steady-state analysis and optimal scheduling of natural gas networks (e.g., the Weymouth equation). For example, in [29], the volume fraction of hydrogen in HCNG was reflected by adjusting the value of the pipeline transmission factor in the general flow equation. However, whether the equation is still applicable to HCNG networks with complex gas components remains to be verified.

C. Contribution

In this context, we focus on more accurate modeling of HCNG networks in centralized hydrogen blending mode for low-carbon and efficient operation of E-HCNG-IES. A convex relaxation method and an iterative algorithm are proposed for the optimal dispatch of E-HCNG-IES. The main contributions of this paper are summarized as follows:

1) Considering the impact of hydrogen on fluid dynamics, we propose an improved steady-state model with a more accurate pressure drop equation and line pack equation for HCNG networks. Comparison with the general flow model is carried out through two examples.

2) We establish a dispatch model for the E-HCNG-IES, covering the "production-storage-blending-transportation-utilization" link of the HCNG supply chain. The original non-convex dispatch model is reformulated into an MISOCP problem based on second-order cone (SOC) relaxation and piecewise linearization techniques.

3) An iterative algorithm based on the convex-concave procedure and bound-tightening method is proposed for the dispatch model to obtain a tight solution.

4) Case studies based on a 6 bus-6 node E-HCNG-IES and a 24 bus-20 node E-HCNG-IES are carried out to validate the effectiveness of the proposed methodology, as well as the impact of hydrogen injection on energy delivery capacity and line pack flexibility of gas networks.

D. Organization

The rest of this paper is organized as follows: Section II presents the improved HCNG network model. Section III proposes the optimal dispatch model for the E-HCNG-IES. The penalty function-bound tightening model and iterative solving algorithm are presented in Section IV. Case studies and conclusions are given in Section V and VI, respectively.

II. An Improved Model of HCNG Network

In this section, the HCNG network model is reformulated by considering the influence of gas components on fundamental equations of gas dynamics, which is then compared with the traditional general flow model through two examples.

A. HCNG Network Modeling

If convection and inertia terms are omitted, equation (1), which describes the one-dimensional steady-state isothermal gas flow, can be replaced by (2).

$$\frac{\partial(\rho v)}{\partial t}+\frac{\partial(\rho v^2)}{\partial x}=-\frac{\partial p}{\partial x}-g\rho\sin\theta-\frac{\lambda v^2}{2D}\rho \tag{1}$$

$$\frac{\partial p}{\partial x}+\frac{\lambda v^2}{2D}\rho=0 \tag{2}$$

Most existing studies on HCNG use volume fraction to describe the proportion of hydrogen in HCNG. Thus, (2) can be transformed to (5) by considering the equation of state of real gases (3) and density equation (4).

$$\rho=\frac{pM}{ZRT} \tag{3}$$

$$m=\rho vA=\rho q \tag{4}$$

$$\frac{\mathrm{d}p}{\mathrm{d}x}+\frac{\lambda M}{2DRTA^2}\frac{p}{Z}\tilde{q}|\tilde{q}|=0 \tag{5}$$

As for a mixture with N_m gas species, the average molecular mass of gas M can be expressed by (6) [37]:

$$M=\sum_{c=1}^{N_m}r_cM_c \tag{6}$$

Unlike natural gas, the compressibility factor Z of HCNG is no longer a constant, and its value is related to the hydrogen volume fraction r_{HCNG} and pressure level p under the assumption of isothermal conditions. According to [18], when hydrogen volume fraction is less than 50%, the linear equation (7) can express the relationship between Z and p.

$$Z=\alpha p+\beta \tag{7}$$

where α and β are parameters related to r_{HCNG}. The unit of α is Pa^{-1} and β is dimensionless. The detailed calculation process can be seen in [18].

Figure 1 presents the linear regression results of Z at $T_{\mathrm{em}}=288.15$ K and $r_{\mathrm{HCNG}}=20\%$. The grey dot represents the actual value of Z, while the purple shading is the deviation of the approximate value from the actual value.

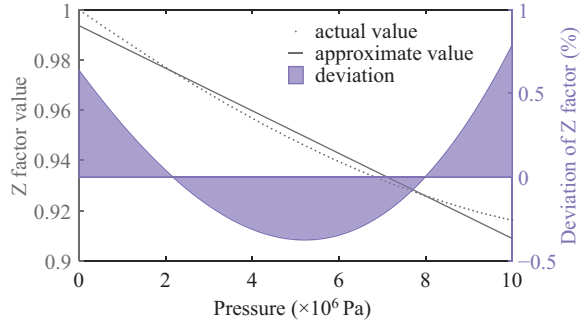

Fig. 1. Linear regression of Z ($T_{\mathrm{em}}=288.15$ K and $r_{\mathrm{HCNG}}=20\%$).

The values of α and β corresponding to Fig. 1 are -8.44×10^{-9} and 0.99337, respectively, and the average deviation level is about 0.29%, which is within the acceptable range.

Based on (7), (5) can be further transformed to (8):

$$\frac{\mathrm{d}p}{\mathrm{d}x}+\frac{\lambda M}{2DRTA^2}\frac{p}{\alpha p+\beta}\tilde{q}|\tilde{q}|=0 \tag{8}$$

Integrate (8) between the upstream side ($x=0, p=p_i$) and the downstream side ($x=L_{ij}, p=p_j$) of pipeline ij, and (9) is obtained:

$$p_{i,t}-p_{j,t}+\frac{\beta}{\alpha}(\ln p_{i,t}-\ln p_{j,t})=\frac{\lambda M L_{ij}}{2DRTA^2\alpha}\tilde{q}_{ij,t}|\tilde{q}_{ij,t}|,\forall ij,t \tag{9}$$

where $\tilde{q}_{ij,t}=(q^{\mathrm{in}}_{ij,t}+q^{\mathrm{out}}_{ij,t})/2$.

The logarithmic terms in (9) are piecewise linearized on the interval $[p_{\min},p_{\max}]$. The bilinear terms are linearized on the interval $[\tilde{q}_{\min},\tilde{q}_{\max}]$ by the special ordered sets 2 (SOS2) method to compare with the general flow model in Section II-B, while a more efficient method is adopted in Section IV. See [38] for the specific process of piecewise linearization and SOS2 methods.

The HCNG network must comply with nodal energy conservation, which is denoted by (10):

$$LHV_{\mathrm{HCNG}}\left(\sum_{w\to i}q_{w,t}+\sum_{j\to i}q^{\mathrm{out}}_{ij,t}-\sum_{j\to i}q^{\mathrm{in}}_{ij,t}-\sum_{gt\to i}q_{gt,t}\right)\cdot 3600/1000=L^{\mathrm{G}}_{i,t},\ \forall i,t \tag{10}$$

where $LHV_{\mathrm{HCNG}}=r_{\mathrm{HCNG}}LHV_H+(1-r_{\mathrm{HCNG}})LHV_{\mathrm{NG}}$; $q_{w,t}$ and $q^{\mathrm{out}}_{ij,t}$ represent gas injection from source nodes and upstream pipelines connected to node i; $q^{\mathrm{in}}_{ij,t}$ and $q_{gt,t}$ represent gas flowing out of node i to its downstream pipelines and gas turbines; $L^G_{i,t}$ denotes gas loads in the unit of MW; the arrow symbol denotes the case where the index node is connected to node i.

Gas flow rate from source nodes and pressure of each node are constrained by their upper and lower limits, as shown in (11) and (12):

$$q_{w,\min}\le q_{w,t}\le q_{w,\max},\ \forall w,t \tag{11}$$

$$p_{i,\min}\le p_{i,t}\le p_{i,\max},\ \forall i,t \tag{12}$$

Gas inertia enables pipelines to store energy, called line pack or line bagging. Line pack is determined by physical parameters and average pressure of the pipeline, which is denoted by (13) and (14) [39]:

$$\tilde{S}_{ij,t}=\frac{A_{ij}L_{ij}T_n}{p_nT}\frac{\tilde{p}_{ij,t}}{Z},\ \forall ij,t \tag{13}$$

$$\tilde{S}_{ij,t}=\tilde{S}_{ij,t-1}+(q^{\mathrm{in}}_{ij,t}-q^{\mathrm{out}}_{ij,t})\Delta t,\ \forall ij,t \tag{14}$$

where $\tilde{p}_{ij,t}=(p_{i,t}+p_{j,t})/2$.

When considering HCNG as the gas medium, Z in (13) can be replaced by $\tilde{Z}=\alpha\tilde{p}+\beta$, then (13) can be transformed to (15):

$$\frac{\alpha p_nT}{ALT_n}\tilde{S}_{ij}(p_i+p_j)+\frac{2\beta p_nT}{ALT_n}\tilde{S}_{ij}=(p_i+p_j),\ \forall ij,t \tag{15}$$

In addition, the total line pack of an HCNG network should be restored to the initial value periodically to facilitate periodic dispatch.

$$\sum_{t\in N_t}\sum_{ij\in\Omega_{\text{pipe}}}\tilde{S}_{ij,t}=\sum_{ij\in\Omega_{\text{pipe}}}\tilde{S}_{ij,1} \tag{16}$$

So far, the improved HCNG network model has been formulated by (9)–(12), and (14)–(16).

B. Comparison with General Flow Model

In the traditional general flow equation, compressibility factor Z is regarded as a constant, pressure drop equation is expressed as (17), and line pack equation has been shown in (13).

$$\left(\frac{\pi}{4}\right)^2\frac{D_{ij}^5RT_n^2}{\lambda L_{ij}p_n^2MZT}(p_{i,t}^2-p_{j,t}^2)=\tilde{q}_{ij}|\tilde{q}_{ij}|,\ \forall ij,t \tag{17}$$

where the bilinear terms in (17) will also be linearized by the method of SOS2 [38].

To illustrate the impact of blending hydrogen with natural gas on gas network dispatch under different pressure levels, a 37-node gas network at 2 bar and a 6-node gas network at 60 bar are taken as examples. Their topologies are shown in Fig. 2. The network parameters, load data, and economic parameters can be seen in [40].

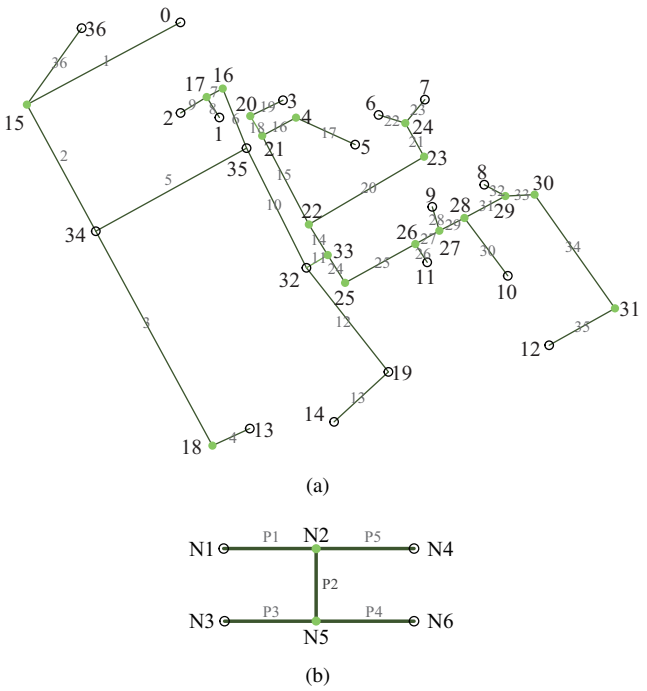

Fig. 2. Gas network topologies of two examples. (a) 37-node gas network. (b) 6-node gas network.

The dispatch model using the general flow model (M0) and the improved HCNG network model (M1) are presented in (18) and (19), respectively. It can be seen that the optimization objective of the two models is to minimize the daily HCNG cost, while differences appear in their operational constraints.

$$\begin{cases}\min C_{\text{HCNG}}=\sum_{t\in N_t}\left(k_{\text{HCNG},t}^{\text{buy}}V_{\text{HCNG},t}^{\text{buy}}\right)\cdot 3600\Delta t\\ \textit{s.t.}\ (9)\text{–}(14),\ (16),\ (17)\end{cases} \tag{18}$$

$$\begin{cases}\min C_{\text{HCNG}}=\sum_{t\in N_t}\left(k_{\text{HCNG},t}^{\text{buy}}V_{\text{HCNG},t}^{\text{buy}}\right)\cdot 3600\Delta t\\ \textit{s.t.}\ (9)\text{–}(12),\ (14)\text{–}(16)\end{cases} \tag{19}$$

After being linearized by SOS2, the dispatch models are programmed by MATLAB R2021b and solved by YALMIP + Cplex (Version 12.8.0).

In the following case studies, the r_{HCNG} value of the two topologies shown in Fig. 2 varies from 0 to 20% with a step of 1%. Fig. 3 shows the optimization results of the objective function under the two models, where the grey line represents the 2-bar scenario, and the purple line represents the 60-bar scenario. Taking the optimization result obtained by the improved HCNG network model as the reference value, the deviation of the optimization result obtained by the general flow model relative to it is obtained.

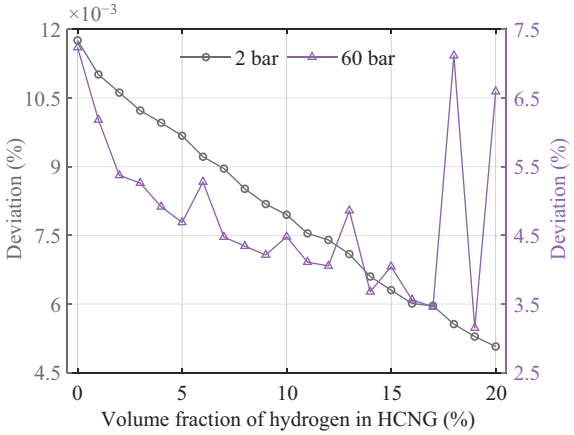

Fig. 3. Deviation of the optimization results of the objective function.

Specifically, the average deviation in the 2-bar scenario is about 0.008%, while that in the 60-bar scenario is around 4.81%. The latter is 601.25 times that of the former, indicating that the impact of blending hydrogen with natural gas on the high-pressure gas network is much greater than that on the low-pressure gas network.

Taking the 60-bar scenario with $r_{\text{HCNG}}=20\%$ as an example, Fig. 4(a) and (b) present the optimization results of the pressure of selected nodes and HCNG flow rate of selected pipelines under the two models. The dashed line represents the general flow model (M0), while the solid line represents the improved HCNG network model (M1). It can be seen that the network operating conditions obtained by the two models are significantly different.

In general, assuming that r_{HCNG} is determined for an HCNG network at high-pressure level, fluctuation of the Z caused by pressure changes cannot be ignored. If the general flow model is still used for HCNG network optimal dispatch at high pressure, it will cause non-negligible deviations. Both the improved HCNG network model and the general flow model contain bilinear terms, and the former also introduces logarithmic terms, which can be regarded as the price paid for considering the impact of pressure variation on Z. A more accurate and efficient solution method for dealing with bilinear and logarithmic terms is given in Section IV.

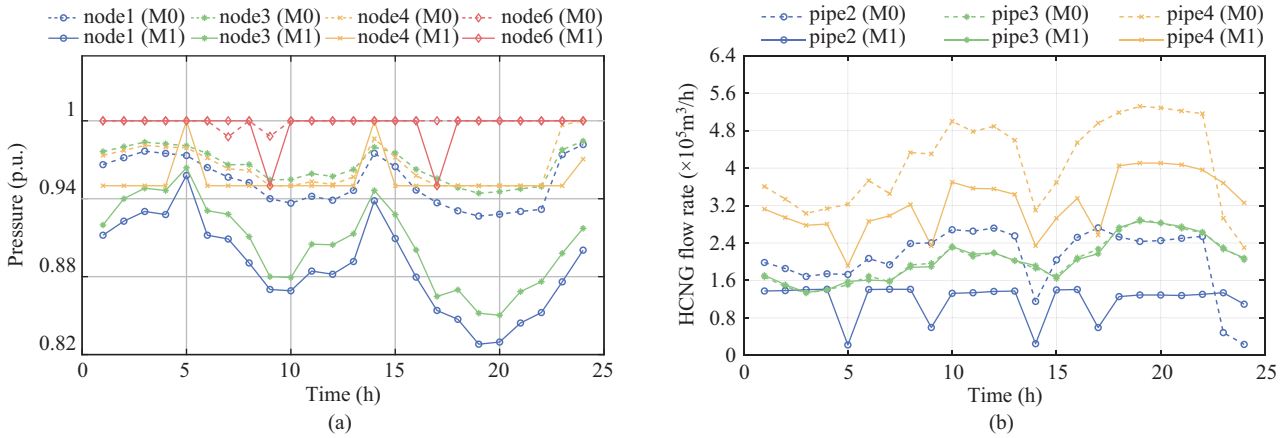

Fig. 4. Comparison of the optimization results of network operation conditions. (a) Node pressure. (b) HCNG flow rate.

III. Optimal Dispatch Model for E-HCNG-IES

This section constructs a dispatch model for the E-HCNG-IES. As shown in Fig. 5, the "production-storage-blending-transportation-utilization" link of the HCNG supply chain is briefly introduced as follows.

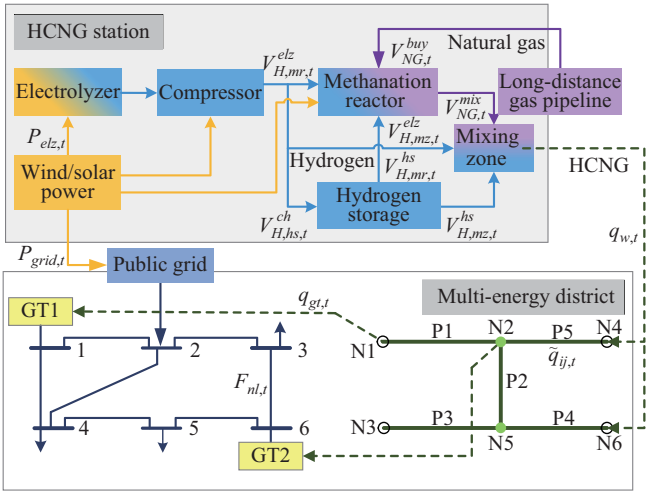

Fig. 5. Schematic diagram of E-HCNG-IES structure.

The centralized HCNG station gathers functions, including renewable energy generation, hydrogen production, compression, storage, methanation, and blending. Abundant renewable energy generation near the HCNG station, including wind and solar power, has two destinations: one is to supply downstream power users via the public grid, and the other is to satisfy equipment in the HCNG station, including the electrolyzer (ELZ), compressor (CP) and methanation reactor (MR) [41]. After being compressed by the CP, hydrogen produced by water electrolysis can be stored in hydrogen storage (HS) facilities, injected into the MR for conversion into synthetic natural gas, or directly injected into the mixing zone (MZ) to prepare HCNG [42]. When hydrogen demand peaks, hydrogen can be withdrawn from HS to supply MR and MZ. It should be noted that the upstream long-distance gas pipeline is still the primary gas source of the HCNG station. The HCNG outflow from the mixing zone is injected into the multi-energy district and transported by the HCNG network to satisfy gas and electric loads, including industrial, commercial and residential users. In addition, the HCNG and electricity network in the multi-energy district are coupled by gas-to-power units.

The centralized hydrogen blending mode in Fig. 5 can apply to the early stage of HCNG development and promotion, supporting operation of centralized HCNG demonstration projects and utilization of HCNG in local IES.

A. Objective Function

The objective of the E-HCNG-IES dispatch is to minimize daily operation cost, as shown in (20) to (25).

$$\min C_{tot} = \sum_{t\in N_t}\Big(C_{NG,t} + C^{\mathrm{CO_2}}_{\mathrm{penal},t} + C^{\mathrm{RES}}_{\mathrm{curt},t} + C_{om,t} + C_{\mathrm{wheel},t}\Big) \tag{20}$$

$$C_{NG,t} = k^{\mathrm{buy}}_{NG,t} V^{\mathrm{buy}}_{NG,t} \cdot 3600\Delta t \tag{21}$$

$$C^{\mathrm{CO_2}}_{\mathrm{penal},t} = penal^{\mathrm{CO_2}}_{\mathrm{NG}} V^{\mathrm{buy}}_{NG,t} \cdot 3600\Delta t \tag{22}$$

$$C^{\mathrm{RES}}_{\mathrm{curt},t} = \Big[penal^{\mathrm{curt}}_{wt}(P^{\mathrm{fore}}_{wt,t} - P_{wt,t}) + penal^{\mathrm{curt}}_{pv}(P^{\mathrm{fore}}_{pv,t} - P_{pv,t})\Big]\Delta t \tag{23}$$

$$C_{om,t} = \Big[k^{gt}_{om}\sum P_{gt,t} + k^{wt}_{om}\sum P_{wt,t} + k^{pv}_{om}\sum P_{pv,t} + k^{elz}_{om}\sum P_{elz,t} + k^{mr}_{om}\sum V_{NG,mr,t}\cdot 3600 + k^{hs}_{om}\sum(V^{ch}_{hs,t} + V^{dis}_{hs,t})\cdot 3600 + k^{mz}_{om}\sum(V^{\mathrm{mix}}_{NG,t} + V^{\mathrm{mix}}_{H,t})\cdot 3600\Big]\Delta t \tag{24}$$

$$C_{\mathrm{wheel},t} = k^{\mathrm{grid}}_{\mathrm{wheel}} P_{\mathrm{grid},t}\Delta t \tag{25}$$

where $C_{\mathrm{NG,t}}$ is natural gas purchasing cost from the long transmission line; $C^{\mathrm{CO_2}}_{\mathrm{penal},t}$ and $C^{RES}_{curt,t}$ are penalties for carbon emission and renewable energy generation curtailment, respectively; $C_{om,t}$ is maintenance costs of devices; $C_{\mathrm{wheel},t}$ is wheeling fees paid to the public grid for electricity transmission from the HCNG station to the multi-energy district.

B. Constraints

Operation constraints of E-HCNG-IES include HCNG network constraints, electricity network constraints, device oper-

ation constraints, and multi-energy flow balance. Constraints except HCNG network constraints are introduced here.

1) Electricity Network

The electricity network is modeled by DC power flow in this paper, as shown in (26) to (28):

$$\sum_{l\to n} F_{nl,t} + \sum_{gt\to n} P_{gt,t} = L^{E}_{n,t},\ \forall n,t \tag{26}$$

$$F_{nl,t} = \frac{\theta_{n,t} - \theta_{l,t}}{X_{nl}},\ \forall nl,t \tag{27}$$

$$-F_{nl,\max} \le F_{nl,t} \le F_{nl,\max},\ \forall nl,t \tag{28}$$

It should be noted that electricity transmitted from the HCNG station to the multi-energy district must satisfy constraints (29):

$$0 \le P_{\mathrm{grid},t} \le P^{\max}_{\mathrm{grid}},\ \forall t \tag{29}$$

2) Operational Constraints of GT

According to [43], with 10% hydrogen blended into natural gas, gas turbines' (GTs') CO and NO emissions can be reduced by 60% and 14%, respectively. The GTs fueled with HCNG are modeled by (30) to (33) [44]. Since heat load is not considered in this paper, only electrical output of the GT is considered in the optimal scheduling model.

$$\begin{aligned} P_{gt,t} = {} & [3.031\cdot(1-r_{\mathrm{HCNG}})q_{gt,t} \\ & + 1.019\cdot r_{\mathrm{HCNG}} q_{gt,t}]\cdot 3600/1000,\ \forall t \end{aligned} \tag{30}$$

$$\begin{aligned} Q_{gt,t} = {} & [6.086\cdot(1-r_{\mathrm{HCNG}})q_{gt,t} \\ & - 0.5331\cdot r_{\mathrm{HCNG}} q_{gt,t}]\cdot 3600/1000,\ \forall t \end{aligned} \tag{31}$$

$$P^{\min}_{gt} \le P_{gt,t} \le \mathit{Cap}_{gt}, \forall t \tag{32}$$

$$-\mathit{ramp}^{\max}_{gt}\cdot\Delta t \le P_{gt,t} - P_{gt,t-1} \le \mathit{ramp}^{\max}_{gt}\cdot\Delta t, \forall t \tag{33}$$

3) Renewable Energy Generation

According to [45], theoretical power output of a wind turbine (WT) can be calculated by (34), and actual utilized wind power is constrained by (35).

$$P^{\mathrm{fore}}_{wt,t} = 0.5\times 10^{-6}\times\pi\eta_{wt}\rho_{air}N_{wt}R^{2}_{wt}(u_t)^3,\ \forall t \tag{34}$$

$$0 \le P_{wt,t} \le P^{\mathrm{fore}}_{wt,t},\ \forall t \tag{35}$$

Theoretical power output of photovoltaic (PV) panels is characterized by (36), and actual utilized solar power is limited by (37) [46].

$$P^{\mathrm{fore}}_{pv,t} = \Re_t \cos\theta_{pv}\eta_{\mathrm{MPPT}}A_{pv}\eta_{pv}/1000,\ \forall t \tag{36}$$

$$0 \le P_{pv,t} \le P^{\mathrm{fore}}_{pv,t},\ \forall t \tag{37}$$

4) Operational Constraints of ELZ, MR, and HS

As shown in (38), compressed hydrogen from the ELZ has three destinations: one is to enter the MZ directly, the second is to be stored in the HS, and the third is to enter the MR to be converted into methane [41].

$$\begin{aligned} \eta_{elz}P_{elz,t} = {} & \mathit{LHV}_H(V^{elz}_{H,mz,t} + V^{ch}_{H,hs,t} + V^{elz}_{H,mr,t}) \\ & \cdot 3600/1000,\ \forall t \end{aligned} \tag{38}$$

Input power of ELZ is constrained by (39):

$$0 \le P_{elz,t} \le \mathit{Cap}_{elz},\ \forall t \tag{39}$$

As shown in (40) and (41), output gas flow from MR is produced from two hydrogen sources, namely the HS and ELZ. Production of MR is also constrained by (42) [47].

$$V^{elz}_{NG,mr,t} = \eta_{mr}V^{elz}_{H,mr,t}\mathit{LHV}_H/\mathit{LHV}_{\mathrm{NG}},\ \forall t \tag{40}$$

$$V^{hs}_{NG,mr,t} = \eta_{mr}V^{hs}_{H,mr,t}\mathit{LHV}_H/\mathit{LHV}_{\mathrm{NG}},\ \forall t \tag{41}$$

$$0 \le \gamma_{mr}(V^{elz}_{NG,mr,t} + V^{hs}_{NG,mr,t})\cdot 3600/1000 \le \mathit{Cap}_{mr},\ \forall t \tag{42}$$

The HS is equipped in the HCNG station to cope with the intermittency of wind and solar power, which is considered pressurized storage vessels and modeled by (43) to (48) in this paper. If geographical conditions permit, hydrogen can also be stored in depleted oil/gas fields or salt caverns, the model of which can be seen in [48].

$$S_{hs,1} = S_{hs,T} = 0.5\cdot\mathit{Cap}_{hs} \tag{43}$$

$$\begin{aligned} S_{hs,t} = {} & S_{hs,t-1}(1-\sigma_{hs}) + (V^{ch}_{H,hs,t}\eta_{hs,ch} - V^{dis}_{H,hs,t}/\eta_{hs,dis}) \\ & \cdot 3600\Delta t, \forall 2 \le t \le N_t \end{aligned} \tag{44}$$

$$V^{dis}_{H,hs,t} = V^{hs}_{H,mr,t} + V^{hs}_{H,mz,t}, \forall t \tag{45}$$

$$\begin{aligned} \mu_{hs,\min}\mathit{Cap}_{hs} \le S_{hs,t} \le \mu_{hs,\max}\mathit{Cap}_{hs}, \\ \forall 2 \le t \le N_t - 1 \end{aligned} \tag{46}$$

$$0 \le V^{ch}_{H,hs,t} \le \gamma_{hs,ch}\mathit{Cap}_{hs}, \forall t \tag{47}$$

$$0 \le V^{dis}_{H,hs,t} \le \gamma_{hs,dis}\mathit{Cap}_{hs}, \forall t \tag{48}$$

5) Multi-energy Flow Balance

The HCNG station also needs to meet a multi-energy balance, and the electricity balance is modeled by (49).

$$\begin{aligned} P_{wt,t} + P_{pv,t} = {} & P_{\mathrm{grid},t} + P_{elz,t}(1+\gamma_{cp}) \\ & + \gamma_{mr}(V^{elz}_{NG,mr,t} + V^{hs}_{NG,mr,t})\cdot 3600/1000,\ \forall t \end{aligned} \tag{49}$$

The natural gas balance constraint and the purchase limit are modeled by (50) and (51), respectively.

$$V^{elz}_{NG,mr,t} + V^{hs}_{NG,mr,t} + V^{\mathrm{buy}}_{NG,t} = V^{\mathrm{mix}}_{NG,t},\ \forall t \tag{50}$$

$$0 \le V^{\mathrm{buy}}_{NG,t} \le V^{\mathrm{buy,max}}_{\mathrm{NG}},\ \forall t \tag{51}$$

Total hydrogen injected into MZ is expressed by (52):

$$V^{elz}_{H,mz,t} + V^{hs}_{H,mz,t} = V^{\mathrm{mix}}_{H,t}, \forall t \tag{52}$$

Gas components in MZ should meet the hydrogen volume fraction requirement and energy conservation law, shown in (53) and (54).

$$V^{\mathrm{mix}}_{H,t} = r_{\mathrm{HCNG}}(V^{\mathrm{mix}}_{H,t} + V^{\mathrm{mix}}_{NG,t}), \forall t \tag{53}$$

$$\mathit{LHV}_H V^{\mathrm{mix}}_{H,t} + \mathit{LHV}_{\mathrm{NG}}V^{\mathrm{mix}}_{NG,t} = \mathit{LHV}_{\mathrm{HCNG}}\sum q_{w,t}, \forall t \tag{54}$$

In conclusion, the MINCQCP model (P0) for the optimal dispatch of E-HCNG-IES is summarized as (55):

$$\begin{cases} \min C_{tot} \\ \textit{s.t.}\ (9)\text{–}(12),\ (14)\text{–}(16),\ (26)\text{–}(30),\ (32)\text{–}(54) \end{cases} \tag{55}$$

where decision variables include: output of energy production devices, input of conversion devices, state of energy storage devices, amount of electricity transmitted by the public grid, amount of natural gas purchased from the upper gas source, flow rate of HCNG injected into the multi-energy district, node pressure, pipeline flow rate and line pack of HCNG network, and power flow and phase angle of electricity network.

C. Evaluation Indicators of HCNG Network Performance

According to theoretical derivation and calculation in [9], blending of hydrogen with natural gas will weaken the pipeline energy delivery capacity and line pack flexibility of the HCNG network, and the weakening effect will deteriorate with the increase of pressure level and hydrogen volume fraction. Combined with core variables in the proposed dispatch model, the following two indicators are defined to evaluate the performance of the HCNG network, which supports the comparative analysis in Section V.

1) Relative Energy Delivery Capacity

In this paper, scenarios with different r_{HCNG} values must meet the same gas load measured in the unit of MW, as shown in (10). Therefore, within the same pressure fluctuation range, the scenario with larger r_{HCNG} needs higher gas flow rates to meet loads of the same scale. Therefore, average energy delivery capacity can be reflected by average gas flow rate concept, which is defined as average value of the flow rate of all pipelines within a dispatch cycle. To be specific, under the same load, the larger the average gas flow rate, the weaker the average energy delivery capacity.

Taking the average gas flow rate of S1 as the reference value, ratios of the other scenarios to S1 are called the relative energy delivery capacity, denoted as Γ_{Sk} in (56).

$$\Gamma_{S_k}=\left[1-\frac{\mathrm{mean}_{S_k}(\tilde{q}_{ij,t})-\mathrm{mean}_{S_1}(\tilde{q}_{ij,t})}{\mathrm{mean}_{S_1}(\tilde{q}_{ij,t})}\right]\times 100\%,\quad \forall ij\in\Omega_{\mathrm{pipe}},\ \forall t\in N_t,\ \forall S_k\in\{S_2,\cdots,S_{N_k}\} \tag{56}$$

where "mean" refers to taking the average value; S_k denotes the k-th sub-scenario of total N_k scenarios.

2) Relative Line Pack Flexibility

In this paper, average line pack flexibility of the HCNG network is defined as average peak shaving capacity of all pipelines, which is characterized by the ratio of peak-valley difference of line pack to valley value and denoted as $LP_{\mathrm{flexi},Sk}$ in (57).

$$LP_{\mathrm{flexi},S_k}=\mathrm{mean}_{S_k}\left[\frac{\max_{S_k}(\tilde{S}_{ij,t})-\min_{S_k}(\tilde{S}_{ij,t})}{\min_{S_k}(\tilde{S}_{ij,t})}\right]\quad \forall ij\in\Omega_{\mathrm{pipe}},\ \forall t\in N_t,\ \forall S_k\in\{S_1,S_2,\cdots,S_{N_k}\} \tag{57}$$

Similar to relative energy delivery capacity concept, relative line pack flexibility is also the comparative value concept, denoted as Ψ_{Sk} in (58).

$$\Psi_{S_k}=\frac{LP_{\mathrm{flexi},S_k}}{LP_{\mathrm{flexi},S_1}}\times 100\%,\ \forall S_k\in\{S_2,\cdots,S_{N_k}\} \tag{58}$$

where "max" and "min" refer to taking the maximum value and minimum value, respectively.

IV. Solution Algorithm

This section introduces the method of converting the original MINCQCP model to a MISOCP one.

A. Second-Order Conic Relaxation

With second-order conic (SOC) relaxation, bilinear terms $\tilde{q}_{ij}|\tilde{q}_{ij}|$ in (9), $\tilde{S}_{ij}p_i$ and $\tilde{S}_{ij}p_j$ in (15) are transformed to (59).

$$\begin{cases}\left\|\begin{matrix}\tilde{S}+\zeta p\\ 1-\zeta\varpi_1\end{matrix}\right\|_2\le 1+\zeta\varpi_1,\ \left\|\begin{matrix}\tilde{S}-\zeta p\\ 1-\zeta\varpi_2\end{matrix}\right\|_2\le 1+\zeta\varpi_2\\ \left\|\begin{matrix}2\tilde{q}\\ 1-\vartheta\end{matrix}\right\|_2\le 1+\vartheta\end{cases} \tag{59}$$

where ϖ_1, ϖ_2, and ϑ are auxiliary variables; ζ is the introduced parameter to ensure $\tilde{S}$ and ζp are close in order of magnitude, thereby avoiding numerical problems.

To reduce the error caused by SOC relaxation, the McCormick envelope is also introduced, as shown in (60).

$$\begin{cases}\varpi\ge\tilde{S}_{\min}p+\tilde{S}p_{\min}-\tilde{S}_{\min}p_{\min},\\ \quad\varpi\ge\tilde{S}_{\max}p+\tilde{S}p_{\max}-\tilde{S}_{\max}p_{\max}\\ \varpi\le\tilde{S}_{\max}p+\tilde{S}p_{\min}-\tilde{S}_{\max}p_{\min},\\ \quad\varpi\le\tilde{S}_{\min}p+\tilde{S}p_{\max}-\tilde{S}_{\min}p_{\max}\\ \vartheta\le(\tilde{q}_{\min}+\tilde{q}_{\max})\tilde{q}-\tilde{q}_{\min}\tilde{q}_{\max}\end{cases} \tag{60}$$

By adding constraints (59) and (60), the MINCQCP model (P0) has been converted to MISOCP (P1) hereto.

B. Penalty Model

Since SOC relaxation (59) discards the non-convex constraint (61), the obtained solution for (P1) may be infeasible for (P0).

$$\begin{cases}4\zeta\varpi_1\le(\tilde{S}+\zeta p)^2,\ 4\zeta\varpi_2\le(\tilde{S}-\zeta p)^2\\ \vartheta\le(\tilde{q})^2\end{cases} \tag{61}$$

Therefore, an iterative solving algorithm is further proposed, in which local optimal for (P0) can be obtained by considering the penalty term in the objective function.

Taking the first non-convex constraint in (61) as an example, it can be treated as the difference between a linear function $f(\varpi)=4\zeta\varpi$ and a convex function $g(\tilde{S},p)=(\tilde{S}+\zeta p)^2$, as shown in (62) [49]:

$$f(\varpi)-g(\tilde{S},p)\le 0 \tag{62}$$

Obviously, the convex function $g(\tilde{S},p)$ satisfies the constraint in (63):

$$\begin{aligned}g(\tilde{S},p)\ge&\left[g'_{\tilde{S}}(\tilde{S}^{(k)},p^{(k)})(\tilde{S}-\tilde{S}^{(k)})\right.\\&\left.+g'_p(\tilde{S}^{(k)},p^{(k)})(p-p^{(k)})+g(\tilde{S}^{(k)},p^{(k)})\right]\\=&\hat{g}^{(k)}(\tilde{S},p)\end{aligned} \tag{63}$$

where $\hat{g}^{(k)}(\tilde{S},p)$ denotes the tangent plane of $g(\tilde{S},p)$ at $(\tilde{S}^{(k)},p^{(k)})$; $g'_{\tilde{S}}(\tilde{S}^{(k)},p^{(k)})$ and $g'_p(\tilde{S}^{(k)},p^{(k)})$ are partial derivatives of $g(\tilde{S},p)$ to $\tilde{S}$ and p at $(\tilde{S}^{(k)},p^{(k)})$, respectively.

Therefore, (62) can be relaxed to (64):

$$f(\varpi)-\hat{g}^{(k)}(\tilde{S},p)\le s \tag{64}$$

where s is a slack variable that can be added to the objective function as a penalty term to reduce slack error.

The slack form of (61) can be written as (65):

$$\begin{cases} 4\zeta\varpi_1 - \left[2\cdot(\tilde{S}^{(k)}+\zeta p^{(k)})(\tilde{S}+\zeta p) - (\tilde{S}^{(k)}+\zeta p^{(k)})^2\right] \\ \quad \le s_1 \\ 4\zeta\varpi_2 - \left[2\cdot(\tilde{S}^{(k)}-\zeta p^{(k)})(\tilde{S}-\zeta p) - (\tilde{S}^{(k)}-\zeta p^{(k)})^2\right] \\ \quad \le s_2 \\ \vartheta - \left[2\cdot\tilde{q}^{(k)}\tilde{q} - (\tilde{q}^{(k)})^2\right] \le s_3 \\ s_1, s_2, s_3 \ge 0 \end{cases} \tag{65}$$

So far, (P1) is modified into penalty model (P2), as shown in (66):

$$\begin{cases} \min C_{tot} + \kappa^{(k)} s_{\text{sum}} \\ s.t. \quad \begin{pmatrix} \text{(9)–(12), (14)–(16), (26)–(30),} \\ \text{(32)–(54), (59), (60), (65)} \end{pmatrix} \end{cases} \tag{66}$$

where $\kappa^{(k)}$ denotes the penalty coefficient of the kth iteration; the expression of s_{sum} is shown in (67).

$$s_{\text{sum}} = \sum_{\Omega_{\text{node}},\Omega_{\text{pipe}}} (s_1 + s_2) + \sum_{\Omega_{\text{pipe}}} s_3 \tag{67}$$

Through the iterative solution, the objective function of (P2) will converge when stopping criteria (68) and (69) are satisfied.

$$\text{GAP}_1 = 1 - \frac{C_{tot}^{(k)} + \kappa^{(k-1)} s_{\text{sum}}^{(k)}}{C_{tot}^{(k-1)} + \kappa^{(k-1)} s_{\text{sum}}^{(k-1)}} \le \delta_1 \tag{68}$$

$$\text{GAP}_2 = s_{\text{sum}}^{(k)} \le \delta_2 \tag{69}$$

where δ_1 and δ_2 are the tolerance of GAP_1 and GAP_2.

C. Bound-tightening Method

When the segment number is fixed, the accuracy of the piecewise linearization of the logarithmic term $\ln p$ in (9) is influenced by the segment interval. As shown in Fig. 6, the segment number is assumed to be 1, for the point $(p^*, \ln(p^*))$, the linearization accuracy in segment interval $[p_{\min}^{(1)}, p_{\max}^{(1)}]$ is apparently higher than that in $[p_{\min}^{(2)}, p_{\max}^{(2)}]$.

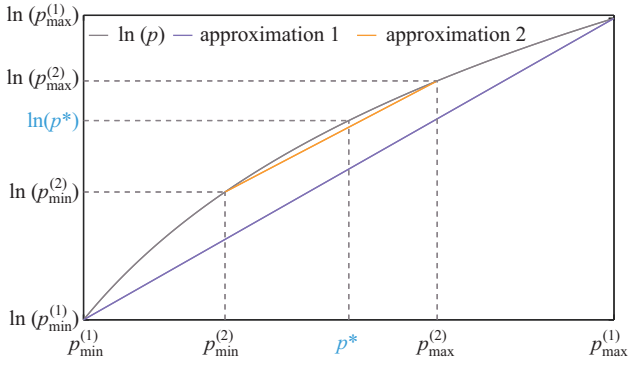

Fig. 6. Piecewise linearization of $\ln p$.

Given this, a bound-tightening method is adopted to improve the linearization accuracy of logarithmic terms [50]. Bound-tightening rules are shown in (70):

$$\begin{cases} p_{\min}^{(k+1)} \leftarrow (1-\varepsilon^{(k)})p^* \\ p_{\max}^{(k+1)} \leftarrow (1+\varepsilon^{(k)})p^* \end{cases} \tag{70}$$

where $\varepsilon^{(k)}$ is the control parameter of bound-tightening, and it is a positive constant less than 1 that monotonically decreases with the increase of iteration number k.

The stopping criterion of bound-tightening is the maximum deviation of the actual value of p from the approximate value, as shown in (71):

$$\text{GAP}_3 = \max_{i\in\Omega_{\text{node}}} \left| \frac{e^{\ln p_i} - p_i}{p_i} \right| \le \delta_3 \tag{71}$$

where δ_3 is the tolerance of GAP_3.

D. Algorithm Flow

Based on the above analysis, the detailed operation process of the proposed iterative algorithm is shown in Fig. 7 [51].

First, initialize parameters related to the number of iterations and tolerance value of each stopping criterion. Next, solve the MISOCP model P1 and obtain solution $(\boldsymbol{p}^{(0)}, \boldsymbol{q}^{(0)}, \tilde{\boldsymbol{S}}^{(0)})$ as initial input of the penalty model P2. In iteratively solving model P2, the algorithm will be terminated if stopping criteria are satisfied. Otherwise, update solution $(\boldsymbol{p}^{(k+1)}, \boldsymbol{q}^{(k+1)}, \tilde{\boldsymbol{S}}^{(k+1)})$, penalty coefficient, and piecewise linearization boundary, and enter the next iteration.

V. Case Studies

This section uses the proposed algorithm to conduct case studies under scenarios with different hydrogen volume fractions. The MISOCP problems in the following case studies are performed on a computer with an i7-9700KF CPU and 32 GB of memory. The programs were developed using MATLAB R2021b and solved by YALMIP + Cplex (Version 12.8.0).

A. System Description

Since the proposed HCNG model is more prominent in gas networks with high pressure, the 6 bus-6 node E-HCNG-IES (gas network at a pressure level of 60 bar) shown in Fig. 5 is selected as the test system in Case I. To compare and analyze influence of different values of r_{HCNG} on operation of E-HCNG-IES, a total of 5 sub-scenarios are set up in this section. Scenario 1 (S1) is the benchmark scenario, and r_{HCNG} is 0. That is, the HCNG station is not considered. From Scenario 2 (S2) to Scenario 5 (S5), r_{HCNG} varies from 5% to 20% with a step of 5%. It is assumed that downstream HCNG consumers can normally use HCNG with r_{HCNG} less than 20%. In order to ensure comparability of these scenarios, their gas loads all adopt energy units. In Case II, a bigger 24 bus-20 node E-HCNG-IES (gas network at a pressure level of 80 bar) is studied.

Configuration of test systems can be seen in [40]. Input parameters of the iteration algorithm are set empirically: $\kappa^{(0)} = 10^6$, $\kappa_{\max} = 2\times10^6$, $\mu = 1.05$, $\delta_1 = 10^{-4}$, $\delta_2 = \delta_3 = 10^{-3}$; $\varepsilon^{(k)} = 0.97^{4k}/2.8$, $K = 50$.

B. Case I

1) Performance of Convergence

Table I compares the computational and convergence performance of S2 to S5.

In these four scenarios where hydrogen is blended with natural gas, the proposed algorithm can converge after 3 to 5

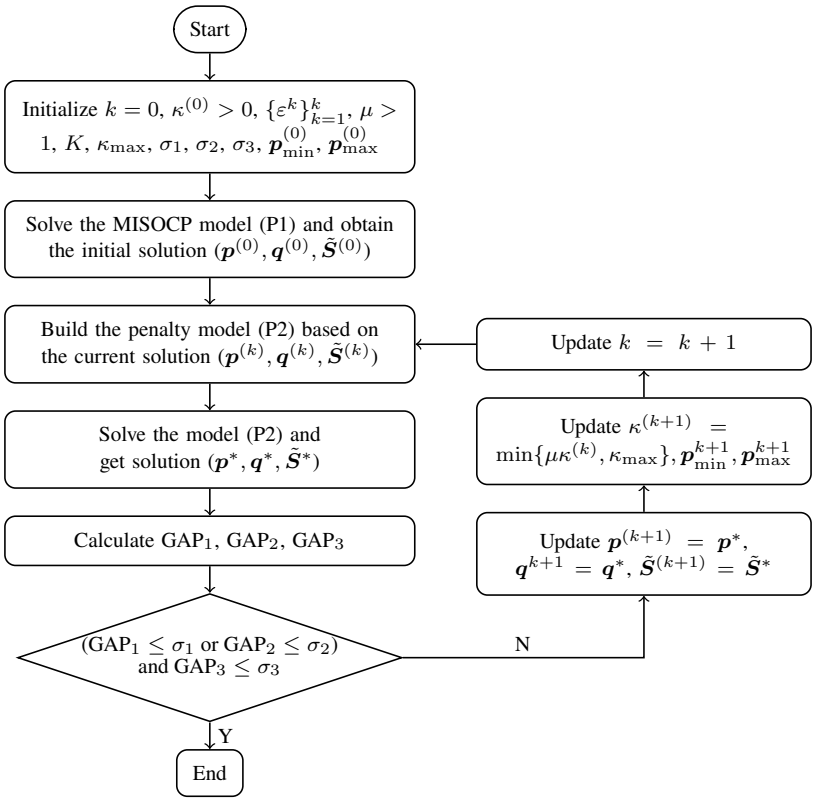

Fig. 7. Procedure of the proposed solving algorithm.

TABLE I
CONVERGENCE PERFORMANCE OF S2 TO S5 IN CASE I

Item		S2	S3	S4	S5
Number of iterations		5	4	3	5
Solver time (s)		2035.94	2501.18	855.56	2369.72
Stopping criteria	GAP_1	6.62×10^{-5}	5.13×10^{-5}	5.17×10^{-5}	5.50×10^{-5}
	GAP_2	1.46×10^{-2}	1.05×10^{-1}	2.30×10^{-2}	5.15×10^{-2}
	GAP_3	3.93×10^{-4}	3.73×10^{-4}	4.33×10^{-4}	4.01×10^{-4}

TABLE II
DISPATCH RESULTS OF S1 TO S5 IN CASE I

Item	S1	S2	S3	S4	S5
Total cost ($\times 10^6$\$)	5.71	5.92	5.90	5.88	5.86
Daily cost of devices maintenance ($\times 10^4$\$)	8.22	90.38	91.39	92.27	93.20
Daily wheeling cost ($\times 10^4$\$)	–	1.31	1.31	1.31	1.31
Daily RES curtailment cost (\$)	–	768.42	0	0	0
Daily natural gas cost ($\times 10^6$\$)	5.16	4.59	4.56	4.54	4.51
Daily CO_2 emission cost ($\times 10^5$\$)	4.66	4.16	4.14	4.12	4.10
Daily CO_2 emission ($\times 10^3$t)	19.52	17.43	17.35	17.26	17.17
Average RES consumption (%)	–	99.67	100	100	100

iterations. The shortest solution time is 855.56 seconds, while the longest solution time is 2501.18 seconds.

2) Economic Analysis

The dispatch results of the five scenarios are listed in Table II.

Since the HCNG station is not included in S1, its daily cost of device maintenance is only less than 10% of that of the other four scenarios. Daily natural gas cost of S1 is 12.4% to 14.4% higher than that of the other four scenarios for not using green renewable energy. At the same time, S1 needs to pay more penalty fees to the carbon trading market for consuming more natural gas. Considering energy loss during energy conversion processes in the HCNG station and relatively low natural gas price, S1 still bears a lower total daily cost, which is about 96.45% of that in S2 and 97.44% of that in S5.

From S2 to S5, system economic performance gradually improves with the increase of r_{HCNG}. Although more hydrogen production means more device maintenance costs in the HCNG station, it can benefit from declining natural gas consumption and carbon emission. When r_{HCNG} reaches 20% in S5, total daily cost of the E-HCNG-IES can be reduced to 98.98% of that in S2, r_{HCNG} of which is 5%. In addition,

with the increase of r_{HCNG}, the E-HCNG-IES's ability to consume renewable energy is also enhanced. In S2, there is a penalty cost of \$768.42 for abandoning wind and solar power, while the E-HCNG-IES can realize 100% renewable energy consumption when r_{HCNG} reaches 10%.

3) Operational Analysis of HCNG Station

Taking S5 as an example, Fig. 8 illustrates operation conditions of devices in the HCNG station when r_{HCNG} is 20%.

As shown in Fig. 8(a), most wind and solar power are used for hydrogen production, compression, and methanation. Due to low cost and zero carbon emissions of renewable energy generation, the HCNG station transmits constant 20 MW power to the multi-energy district during each dispatch period, despite wheeling fees that should be paid to the upper grid. Fig. 8(b) indicates that most natural gas in HCNG comes from the long-distance transmission line, and some natural gas is produced by hydrogen from 0:00 to 9:00 and 12:00 to 17:00. In addition, some hydrogen is withdrawn from the HS for methanation during peak natural gas prices.

In each dispatch period, part of the hydrogen compressed by the CP is directly injected into the MZ to form HCNG, which can be seen in Fig. 8(c). A considerable part of the compressed hydrogen will be used for methanation during peak natural gas prices to reduce purchasing gas from the long-distance transmission line. When natural gas price is low and renewable energy generation is abundant, some hydrogen will be injected into the HS as a reserve.

Operation status of HS is shown in Fig. 8(d). Its hydrogen injection and withdrawal behavior is consistent with the above analysis and shows an effective response to changes in natural gas prices.

4) Operational Analysis of Multi-energy District

Figure 9 illustrates node pressure and pipeline gas flow rate of the HCNG network in S5.

Pressure change of each node in the HCNG network is shown in Fig. 9(a). Among them, pressure of source node 4 and 6 varies from 95% to 100% of the reference value, and pressure of other nodes can be reduced to 73.05% of the reference value during load trough. The pressure change trend of each node is basically the same, which is related to flow rate change trend of the pipelines in Fig. 9(b). Because flow rate of a particular pipeline is determined by the differential pressure between its upstream and downstream sides, as shown in (9).

Line pack change trend of the pipelines is shown in Fig. 10, in which the yellow shadow represents total line pack of the HCNG network, and the area covered by the gray shadow represents periods of low natural gas prices. It can be seen that the HCNG network will release its line pack during peak natural gas prices and accumulate its line pack during low natural gas prices. This behavior reflects the ability of the HCNG network to utilize its gas inertia to respond to varying energy prices, which is also validated in Fig. 11.

As shown in Fig. 11, total HCNG flow rate injected into the multi-energy district is inconsistent with district load. During

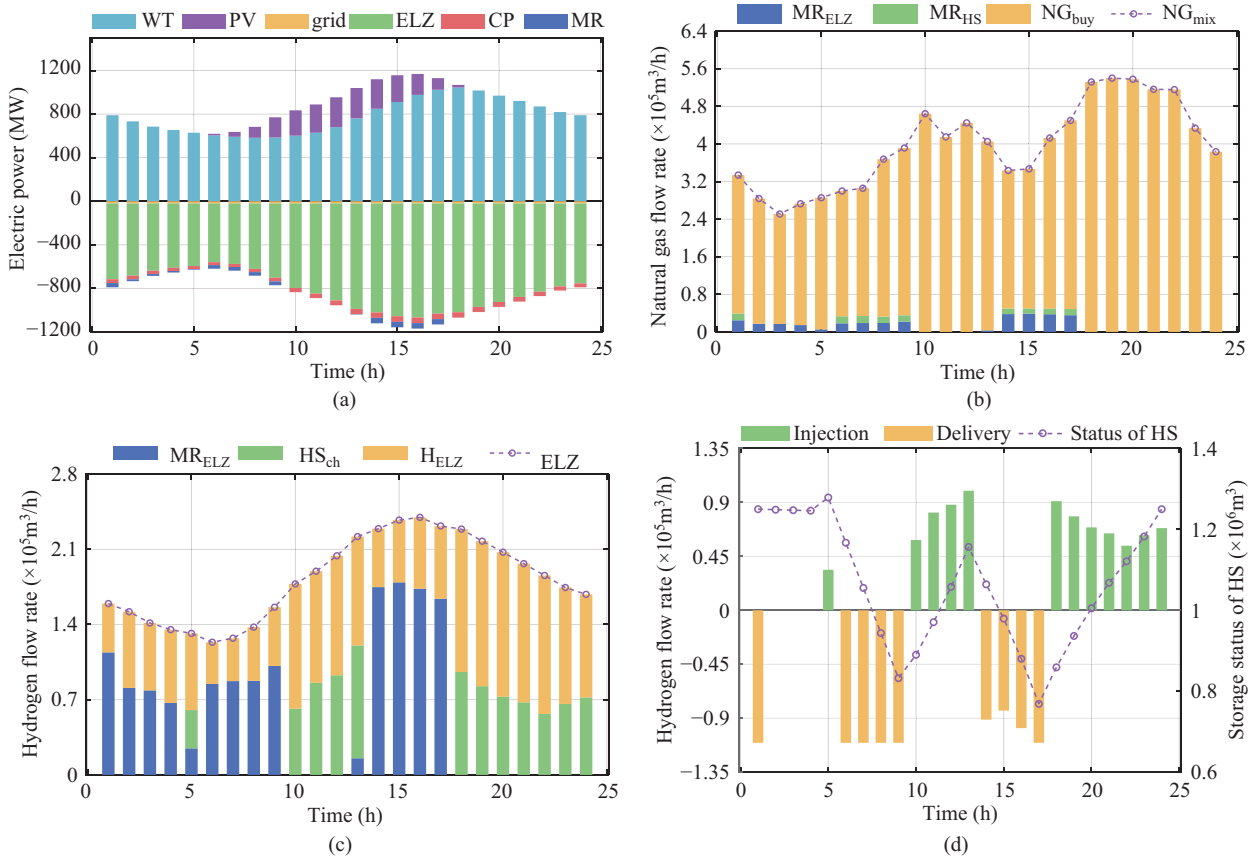

Fig. 8. Operation conditions of devices in the HCNG station in Case I-S5. (a) Electric power balance. (b) Natural gas balance. (c) Hydrogen balance. (d) Operation state of HS.

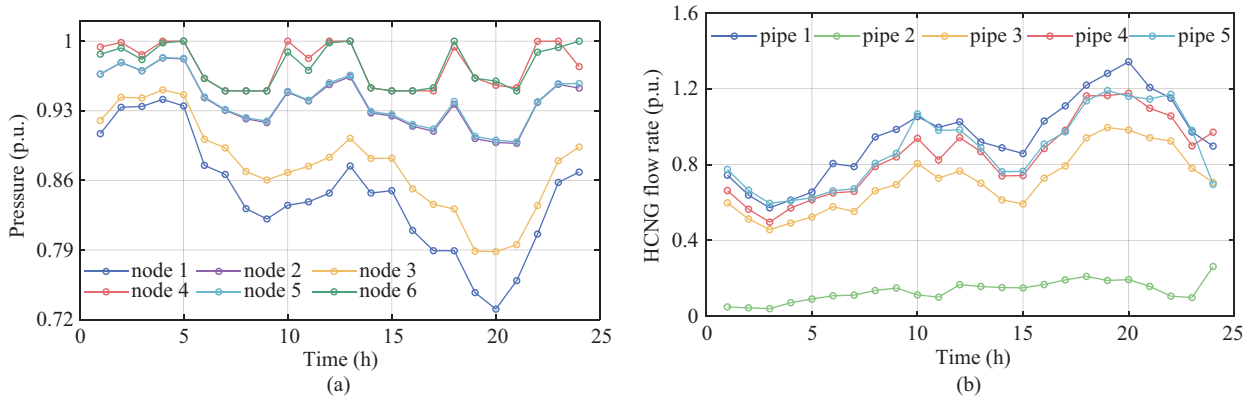

Fig. 9. Operation conditions of the HCNG network in Case I-S5. (a) Node pressure. (b) Pipeline flow rate.

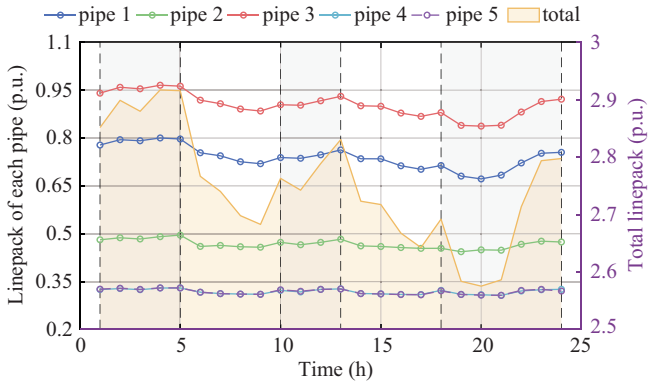

Fig. 10. Line pack of the HCNG network in Case I-S5.

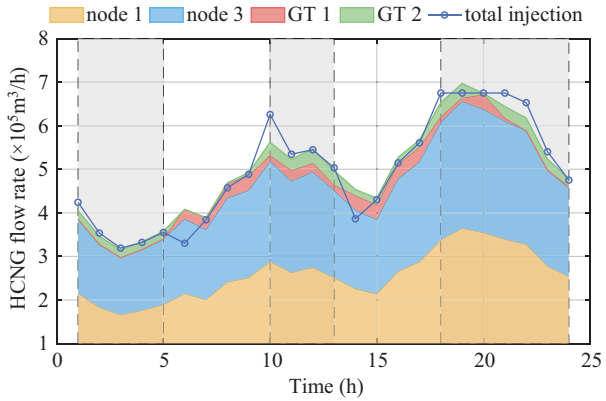

Fig. 11. HCNG flow rate in the HCNG network in Case I-S5.

low natural gas price period, total HCNG injection is more than demand of the multi-energy district, and vice versa in other periods.

5) Comparison of Energy Delivery Capacity and Line Pack Flexibility in HCNG Network

This section quantitatively analyzes the impact of blending hydrogen on the HCNG network from the perspective of energy delivery capacity and line pack flexibility based on dispatch results of Case I. The calculated results of evaluation indicators defined in Section III-C are shown in Table III.

With the increase of hydrogen volume fraction, the energy delivery capacity and line pack flexibility gradually decrease.

TABLE III
ENERGY DELIVERY CAPACITY AND LINE PACK FLEXIBILITY IN CASE I

Item	S1	S2	S3	S4	S5
Average gas flow rate ($\times 10^4$m^3/h)	17.53	18.06	18.81	19.46	20.24
Relative energy delivery capacity, Γ_{Sk} (%)	–	96.98	92.71	88.98	84.54
Average line pack flexibility (%)	15.02	12.85	12.60	12.54	12.26
Relative line pack flexibility, Ψ_{Sk} (%)	–	85.51	83.89	83.43	81.59

Taking S5 as an example, when r_{HCNG} reaches 20%, average energy delivery capacity drops to 84.54% of the reference value, and average line pack flexibility declines to 81.59% of the reference value. Our findings are consistent with the theoretical analysis in [9].

C. Case II

Case II is studied to illustrate the effectiveness and scalability of the proposed method. As shown in Fig. 12, the studied E-HCNG-IES comprises the IEEE 24-bus power system and Belgian 20-node gas system, coupled with 10 gas turbines in this paper. Configuration of the test systems can be seen in [40].

Case II also studies five scenarios, and r_{HCNG} varies from 0% to 20% with a step of 5%. Dispatch results of the five scenarios are listed in Table IV.

TABLE IV
DISPATCH RESULTS OF S1 TO S5 IN CASE II

Item	S1	S2	S3	S4	S5
Total cost ($\times 10^6$\$)	21.41	21.76	21.67	21.57	21.47
Daily cost of devices maintenance ($\times 10^5$\$)	13.06	33.88	34.07	34.29	34.60
Daily wheeling cost ($\times 10^4$\$)	–	6.56	6.56	6.56	6.56
Daily RES curtailment cost (\$)	–	0	0	0	0
Daily natural gas cost ($\times 10^6$\$)	18.42	16.75	16.65	16.53	16.41
Daily CO_2 emission cost ($\times 10^5$\$)	16.94	15.55	15.48	15.41	15.33
Daily CO_2 emission ($\times 10^3$t)	70.94	65.12	64.83	64.52	64.19
Average RES consumption (%)	–	100	100	100	100

The average solver time of S2 to S5 in Case II is 14,399.76 seconds, and the four scenarios all converge after 6 to 9 iterations. It can be seen that the average solver time

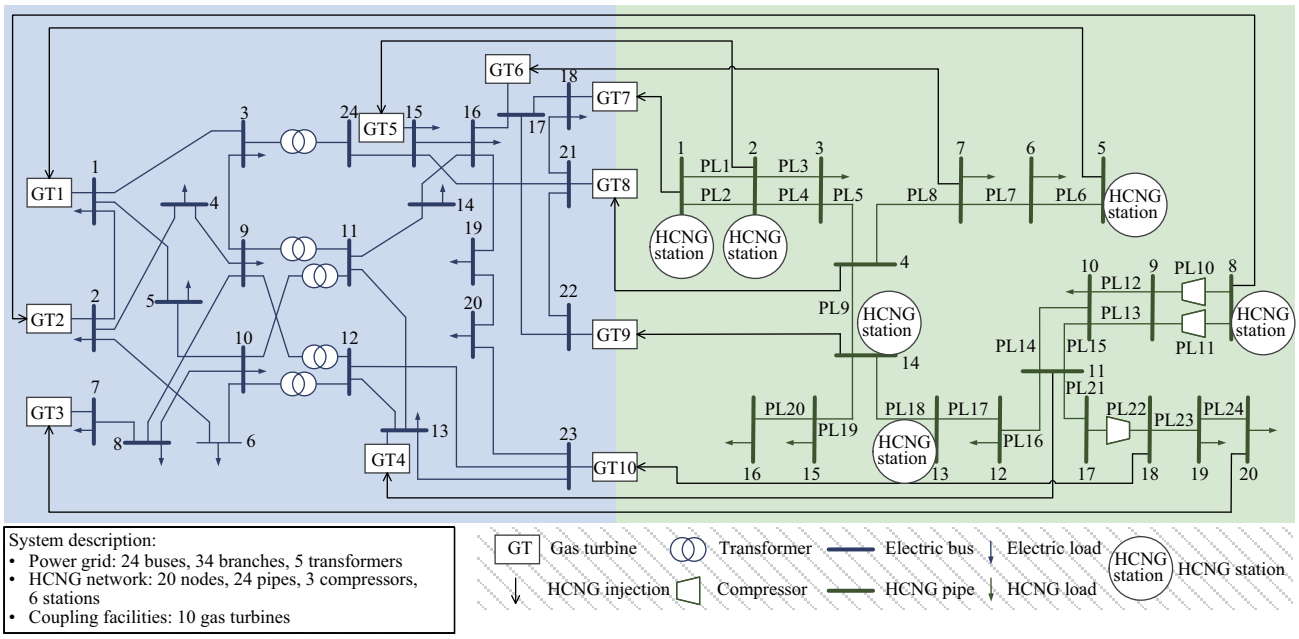

Fig. 12. Topology of E-HCNG-IES in Case II.

of Case II is 7.42 times that of Case I, and the number of iterations is about twice that of Case I. Compared with Case I, the network structure in Case II is more complicated, and the coupling between the electricity and HCNG network is stronger (2 GT units in Case I while 10 GT units in Case II), resulting in higher computational complexity.

Although S1 is the most economical, total daily costs of S2 to S5 decrease with the increase of r_{HCNG} for considering renewable energy use and carbon tax. Detailed operational analysis of the E-HCNG-IES in Case II is similar to that in Case I and is not expanded here.

VI. Conclusion

Considering the impact of hydrogen blending on fundamental equations of gas dynamics, this paper proposes an improved HCNG network model for E-HCNG-IES under centralized hydrogen blending mode. Subsequently, a dispatch model for E-HCNG-IES covering the "production-storage-blending-transportation-utilization" link of the HCNG supply chain is established. The original MINCQCP model is reformulated into a MISOCP model by the SOC relaxation and piecewise linearization techniques. To reduce relaxation errors and obtain a feasible solution, an iterative algorithm combining the convex-concave procedure and bound tightening method is further proposed.

Comparison with the general flow model is first carried out through two examples to illustrate the necessity of the improved HCNG network model. Average deviation of the optimization results of the 60-bar HCNG network reaches 4.81%, which is 601.25 times that of the 2-bar example. Comparison results reveal the significance of considering impact of HCNG on high-pressure gas networks.

Five sub-scenarios based on a 6 bus-6 node E-HCNG-IES are studied in detail to validate the effectiveness of the dispatch model and solving algorithm. Although the benchmark scenario still has certain economic advantages, the economic, environmental, and renewable energy consumption advantages of E-HCNG-IES gradually emerge with incremental hydrogen volume fractions. Specifically, the system can achieve 100% renewable energy consumption when hydrogen volume fraction reaches 10%. When hydrogen volume fraction reaches 20%, daily operating cost can be reduced by 1.02% compared to the 5% scenario. In addition, the influence of hydrogen blending on energy delivery capacity and line pack flexibility of the gas network is verified.

It should be noted that the modelling method and optimal dispatch approach presented in this paper apply to centralized hydrogen blending mode. Since the distributed nature of renewable energy makes decentralized hydrogen blending mode possible in the future, it will be our next research topic.

References

[1] S. Zhang and W. Y. Chen, Assessing the energy transition in China towards carbon neutrality with a probabilistic framework, *Nature Communications*, vol. 13, no. 1, pp. 87, Jan. 2022.

[2] A. E. H. Berjawi, S. L. Walker, C. Patsios, and S. H. R. Hosseini, An evaluation framework for future integrated energy systems: A whole energy systems approach, *Renewable and Sustainable Energy Reviews*, vol. 145, pp. 111163, Jul. 2021.

[3] International Energy Agency, *The future of hydrogen: seizing today's opportunities*, Japan: International Energy Agency, 2019.

[4] H. Zhang, T. J. Yuan, J. Tan, S. J. Kai, and Z. Zhou, Hydrogen energy system planning framework for unified energy system, *Proceedings of the CSEE*, vol. 42, no. 1, pp. 83–93, Jan. 2022.

[5] H. W. Li and N. Nishimiya, Insight from Japan's hydrogen strategy and activities, *Engineering*, vol. 7, no. 6, pp. 722–725, Mar. 2021.

[6] A. Elgowainy, M. Mintz, U. Lee, T. Stephens, P. P. Sun, K. Reddi, Y. Zhou, G. Y. Zang, M. Ruth, P. Jadun, E. Connelly, and R. Boardman, Assessment of potential future demands for hydrogen in the United States, Argonne National Lab. (ANL), Argonne, IL (United States), ANL-20/35 163944, Oct. 2020.

[7] S. Amelang. (2020, Jun. 17). Germany's National Hydrogen Strategy. [Online]. Available: https://www.cleanenergywire.org/factsheets/germanys-national-hydrogen-strategy

[8] H. J. Yoon, S. K. Seo, and C. J. Lee, Multi-period optimization of hydrogen supply chain utilizing natural gas pipelines and byproduct hydrogen, *Renewable and Sustainable Energy Reviews*, vol. 157, pp. 112083, Apr. 2022.

[9] C. J. Quarton and S. Samsatli, Should we inject hydrogen into gas grids? Practicalities and whole-system value chain optimisation, *Applied Energy*, vol. 275, pp. 115172, Oct. 2020.

[10] NaturalHy, Using the existing natural gas system for hydrogen, Project Contract No.: SES6/CT/2004/502661, Oct. 2009.

[11] M. J. Kippers, J. C. D. Laat, and R. J. M. Hermkens, Pilot project on hydrogen injection in natural gas on island of Ameland in the Netherlands, presented at the International Gas Research Conference, 2011.

[12] O. Florisson, HYREADY: engineering guidelines for preparing natural gas networks for hydrogen injection, Brussels: CEN SFEM WG Hydrogen, 2016.

[13] H. G. Zhou. (2019, Oct. 15). The first case in China! The first phase of the HCNG demonstration project by the State Power Investment Corporation Limited was successfully completed. [Online]. Available: http://news.bjx.com.cn/html/20191015/1013148.shtml

[14] J. Shang, W. F. Chen, J. Y. Zheng, Z. L. Hua, L. Zhang, C. S. Zhou, and C. H. Gu, Enhanced hydrogen embrittlement of low-carbon steel to natural gas/hydrogen mixtures, *Scripta Materialia*, vol. 189, pp. 67–71, Dec. 2020.

[15] X. Wu, H. F. Zhang, M. Yang, W. L. Jia, Y. Z. Qiu, and L. Lan, From the perspective of new technology of blending hydrogen into natural gas pipelines transmission: Mechanism, experimental study, and suggestions for further work of hydrogen embrittlement in high-strength pipeline steels, *International Journal of Hydrogen Energy*, vol. 47, no. 12, pp. 8071–8090, Feb. 2022.

[16] C. Wu, Feasibility study on blending hydrogen into natural gas distribution networks, Ph.D. dissertation, Department, Chongqing University, Chongqing, 2018.

[17] Z. Hafsi, S. Elaoud, and M. Mishra, A computational modelling of natural gas flow in looped network: Effect of upstream hydrogen injection on the structural integrity of gas pipelines, *Journal of Natural Gas Science and Engineering*, vol. 64, pp. 107–117, Apr. 2019.

[18] Z. Hafsi, S. Elaoud, M. Akrout, and E. Hadj-Taeb, Numerical approach for steady state analysis of hydrogen–natural gas mixtures flows in looped network, *Arabian Journal for Science and Engineering*, vol. 42, no. 5, pp. 1941–1950, Jan. 2017.

[19] X. H. Li, M. R. Jia, R. R. Zhang, and Z. Y. Han, Dispersion modeling and assessment of natural gas containing hydrogen released from a damaged gas transmission pipeline, *International Journal of Hydrogen Energy*, vol. 47, no. 83, pp. 35365–35385, Oct. 2022.

[20] M. Cavana, A. Mazza, G. Chicco, and P. Leone, Electrical and gas networks coupling through hydrogen blending under increasing distributed photovoltaic generation, *Applied Energy*, vol. 290, pp. 116764, May 2021.

[21] J. Zareei, A. Rohani, F. Mazari, and M. V. Mikkhailova, Numerical investigation of the effect of two-step injection (direct and port injection) of hydrogen blending and natural gas on engine performance and exhaust gas emissions, *Energy*, vol. 231, pp. 120957, Sep. 2021.

[22] M. H. Dinesh, J. K. Pandey, and G. N. Kumar, Study of performance, combustion, and NO_x emission behavior of an SI engine fuelled with ammonia/hydrogen blends at various compression ratio, *International Journal of Hydrogen Energy*, vol. 47, no. 60, pp. 25391–25403, Jul. 2022.

[23] Y. Qiu, S. Y. Zhou, W. Gu, G. S. Pan, and X. G. Chen, Application prospect analysis of hydrogen enriched compressed natural gas technologies under the target of carbon emission peak and carbon neutrality, *Proceedings of the CSEE*, vol. 42, no. 4, pp. 1301–1320, Feb. 2022.

[24] B. Liu, S. X. Liu, S. S. Guo, and S. X. Zhang, Economic study of a large-scale renewable hydrogen application utilizing surplus renewable energy and natural gas pipeline transportation in China, *International Journal of Hydrogen Energy*, vol. 45, no. 3, pp. 1385–1398, Jan. 2020.

[25] P. Danieli, A. Lazzaretto, J. Al-Zaili, A. Sayma, M. Masi, and G. Carraro, The potential of the natural gas grid to accommodate hydrogen as an energy vector in transition towards a fully renewable energy system, *Applied Energy*, vol. 313, pp. 118843, May 2022.

[26] Y. Qiu, S. Y. Zhou, W. Gu, S. X. Ding, G. Y. Han, K. Zhang, and H. K. Lv, Multi-stage flexible planning of regional electricity-HCNG-integrated energy system considering gas pipeline retrofit and expansion, *IET Renewable Power Generation*, vol. 16, no. 15, pp. 3339–3367, Nov. 2022.

[27] Y. J. Song, H. L. Mu, N. Li, and H. Y. Wang, Multi-objective optimization of large-scale grid-connected photovoltaic-hydrogen-natural gas integrated energy power station based on carbon emission priority, *International Journal of Hydrogen Energy*, vol. 48, no. 10, pp. 4087–4103, Feb. 2022.

[28] S. Y. Zhou, K. Y. Sun, Z. Wu, W. Gu, G. X. Wu, Z. Li, and J. J. Li, Optimized operation method of small and medium-sized integrated energy system for P2G equipment under strong uncertainty, *Energy*, vol. 199, pp. 117269, May 2020.

[29] C. Fu, J. Lin, Y. H. Song, J. R. Li, and J. Song, Optimal operation of an integrated energy system incorporated with HCNG distribution networks, *IEEE Transactions on Sustainable Energy*, vol. 11, no. 4, pp. 2141–2151, Oct. 2020.

[30] Z. X. Wang, J. J. Hu, and B. Z. Liu, Stochastic optimal dispatching strategy of electricity-hydrogen-gas-heat integrated energy system based on improved spectral clustering method, *International Journal of Electrical Power & Energy Systems*, vol. 126, pp. 106495, Mar. 2021.

[31] L. Weimann, P. Gabrielli, A. Boldrini, G. Jan Kramer, and M. Gazzani, Optimal hydrogen production in a wind-dominated zero-emission energy system, *Advances in Applied Energy*, vol. 3, pp. 100032, Aug. 2021.

[32] M. Agabalaye-Rahvar, A. Mansour-Saatloo, M. A. Mirzaei, B. Mohammadi-Ivatloo, and K. Zare, Economic-environmental stochastic scheduling for hydrogen storage-based smart energy hub coordinated with integrated demand response program, *International Journal of Energy Research*, vol. 45, no. 14, pp. 20232–20257, Nov. 2021.

[33] S. Zhan, P. Hou, G. Y. Yang, and J. J. Hu, Distributionally robust chance-constrained flexibility planning for integrated energy system, *International Journal of Electrical Power & Energy Systems*, vol. 135, pp. 107417, Feb. 2022.

[34] B. Zhang, W. H. Hu, D. Cao, Q. Huang, Z. Chen, and F. Blaabjerg, Economical operation strategy of an integrated energy system with wind power and power to gas technology–a DRL-based approach, *IET Renewable Power Generation*, vol. 14, no. 17, pp. 3292–3299, Dec. 2020.

[35] Y. C. Tao, J. Qiu, S. Y. Lai, and J. H. Zhao, Integrated electricity and hydrogen energy sharing in coupled energy systems, *IEEE Transactions on Smart Grid*, vol. 12, no. 2, pp. 1149–1162, Mar. 2021.

[36] E. S. Menon, *Gas Pipeline Hydraulics*, Boca Raton: Taylor & Francis Group, 2005.

[37] F. Tabkhi, Optimization of gas transmission networks, Ph.D. dissertation, National Polytechnic Institute of Toulouse, 2007.

[38] M. M. F. Hasan and I. A. Karimi, Piecewise linear relaxation of bilinear programs using bivariate partitioning, *AIChE Journal*, vol. 56, no. 7, pp. 1880–1893, Jul. 2009.

[39] C. M. Correa-Posada and P. Snchez-Martn, Integrated power and natural gas model for energy adequacy in short-term operation, *IEEE Transactions on Power Systems*, vol. 30, no. 6, pp. 3347–3355, Nov. 2015.

[40] Y. Qiu. (2022). Test data of the E-HCNG-IES. Available: https://www.dropbox.com/scl/fi/ftcz64zxibz37fsk3skid/Test-data-of-the-E-HCNG-IES.xlsx?dl=0&rlkey=7d98o6eqvwsnlxqk71nnwwmqe

[41] B. Li, X. Li, and Q. Y. Su, A system and game strategy for the isolated island electric-gas deeply coupled energy network, *Applied Energy*, vol. 306, pp. 118013, Jan. 2022.

[42] L. Kouchachvili and E. Entchev, Power to gas and H_2/NG blend in SMART energy networks concept, *Renewable Energy*, vol. 125, pp. 456–464, Sep. 2018.

[43] S. Meziane and A. Bentebbiche, Numerical study of blended fuel natural gas-hydrogen combustion in rich/quench/lean combustor of a micro gas turbine, *International Journal of Hydrogen Energy*, vol. 44, no. 29, pp. 15610–15621, Jun. 2019.

[44] S. Y. Zhou, D. He, W. Gu, Z. Wu, G. Abbas, Q. T. Hong, and C. Booth, Design and evaluation of operational scheduling approaches for HCNG penetrated integrated energy system, *IEEE Access*, vol. 7, pp. 87792–87807, Jun. 2019.

[45] S. Samsatli, I. Staffell, and N. J. Samsatli, Optimal design and operation of integrated wind-hydrogen-electricity networks for decarbonising the domestic transport sector in Great Britain, *International Journal of Hydrogen Energy*, vol. 41, no. 1, pp. 447–475, Jan. 2016.

[46] M. H. Rahman and S. Yamashiro, Novel distributed power generating system of PV-ECaSS using solar energy estimation, *IEEE Transactions on Energy Conversion*, vol. 22, no. 2, pp. 358–367, Jun. 2007.

[47] G. S. Pan, W. Gu, Y. P. Lu, H. F. Qiu, S. Lu, and S. Yao, Accurate modeling of a profit-driven power to hydrogen and methane plant toward strategic bidding within multi-type markets, *IEEE Transactions on Smart Grid*, vol. 12, no. 1, pp. 338–349, Jan. 2021.

[48] Y. Qiu, S. Y. Zhou, J. H. Wang, J. Chou, Y. H. Fang, G. S. Pan, and W. Gu, Feasibility analysis of utilising underground hydrogen storage facilities in integrated energy system: Case studies in China, *Applied Energy*, vol. 269, pp. 115140, Jul. 2020.

[49] S. Lu, W. Gu, C. Zhang, K. Meng, and Z. Y. Dong, Hydraulic-thermal cooperative optimization of integrated energy systems: a convex optimization approach, *IEEE Transactions on Smart Grid*, vol. 11, no. 6, pp. 4818–4832, Jun. 2020.
[50] S. Chen, A. J. Conejo, R. Sioshansi, and Z. N. Wei, Unit commitment with an enhanced natural gas-flow model, *IEEE Transactions on Power Systems*, vol. 34, no. 5, pp. 3729–3738, Sep. 2019.
[51] W. J. Dong, L. Zhang, D. X. Zhang and Q. S. Cui, "Hierarchical Multi-objective Planning for Integrated Energy Systems in Smart Parks Considering Operational Characteristics," *CSEE Journal of Power and Energy Systems*, vol. 8, no. 6, pp. 1760–1771, Nov. 2022.

Yue Qiu received the B.Eng degree in Electrical Engineering from Nanjing University of Aeronautics and Astronautics, Nanjing, China, in 2018. She is currently pursuing the Ph.D. degree at the School of Electrical Engineering, Southeast University, Nanjing, China. Her research interests include electricity market, modeling, planning and optimization of the integrated energy systems.

Suyang Zhou received the B.Eng. degree from Huazhong University of Science and Technology in 2009 and Ph.D. degree from University of Birmingham in 2015, both in Electrical Engineering. He is now an Associate Professor with School of Electrical Engineering, Southeast University, Nanjing. Prior to joining Southeast University, he worked as KTP associate at University of Leicester and research and development engineer at Cellcare Technology Ltd. between 2015 and 2016, and worked as data scientist at Power Networks Demonstration Centre (a joint research center between University of Strathclyde and UK distribution network operators) between 2016 and 2017. His main research interests include the integrated energy system, artificial intelligence in the electrical domain and demand side management.

Wei Gu received the B.Eng. and Ph.D. degrees in Electrical Engineering from Southeast University, China, in 2001 and 2006, respectively. From 2009 to 2010, he was a Visiting Scholar with the Department of Electrical Engineering, Arizona State University, Tempe, AZ, USA. He is currently a Professor with the School of Electrical Engineering, Southeast University. His research interests include distributed generations and microgrids and active distribution networks.

Yuping Lu received the Ph.D. degree in Electrical Engineering from the City University, U.K., in 2003. He is working as a Professor with the Southeast University of China. His research interests are power system protection, especially digital relaying of generator-transformer unit, and protection and control techniques of distribution system.

Xiao-Ping Zhang received the B.Eng., M.Sc., and Ph.D. degrees in Electrical Engineering from Southeast University, China in 1988, 1990, 1993, respectively. He is currently a Professor in Electrical Power Systems and Director of Smart Grid of Birmingham Energy Institute at the University of Birmingham, U.K. His research interests include modeling and control of HVDC, FACTS, and wind/wave generation, distributed energy systems and market operations, power system planning, global electricity grid, global power and energy Internet, energy union, wind and solar power variability, and energy quality. He has been the Advisor to IEEE PES U.K. and Ireland Chapter and chairing the IEEE PES WG on Test Systems for Economic Analysis. He is appointed recently to the Expert Advisory Group of U.K. Government's Offshore Transmission Network Review. He is an IEEE PES Distinguished Lecturer on HVDC, FACTS, and Wave Energy Generation. He is a Fellow of CSEE and IET. He has been a Fellow of IEEE for contributions to modeling and control of high-voltage DC and AC transmission systems.

Gaoyan Han is a senior engineer at the Electric Power Research Institute of State Grid Zhejiang Electric Power Co., Ltd., engaged in research on technical support related to integrated energy services.

Kang Zhang received the Ph.D. degree from Zhejiang University and is currently a senior engineer at the Electric Power Research Institute of State Grid Zhejiang Electric Power Co., Ltd. He is mainly engaged in the technologies of energy efficiency improvement, carbon capture and utilization, new energy storage, and demand-side response.

Hongkun Lyu received the Ph.D. degree from Zhejiang University in 2009 and is currently the Deputy Director of Energy Technology Center at the Electric Power Research Institute of State Grid Zhejiang Electric Power Co., Ltd. His research interests are energy internet, integrated energy services, and power saving and emission reduction.